

# PathoGen: Diffusion-Based Synthesis of Realistic Lesions in Histopathology Images

Mohamad Koohi-Moghadam<sup>1\*</sup>, Mohammad-Ali Nikouei Mahani<sup>1</sup>, Kyongtae Tyler Bae<sup>1</sup>

<sup>1</sup> Department of Diagnostic Radiology, Li Ka Shing Faculty of Medicine, The University of Hong Kong, Pok Fu Lam, Hong Kong SAR, PR China

Corresponding author: [koohi@hku.hk](mailto:koohi@hku.hk)

## Abstract

The development of robust artificial intelligence models for histopathology diagnosis is severely constrained by the scarcity of expert-annotated lesion data, particularly for rare pathologies and underrepresented disease subtypes. While data augmentation offers a potential solution, existing methods fail to generate sufficiently realistic lesion morphologies that preserve the complex spatial relationships and cellular architectures characteristic of histopathological tissues. Here we present PathoGen, a diffusion-based generative model that enables controllable, high-fidelity inpainting of lesions into benign histopathology images. Unlike conventional augmentation techniques, PathoGen leverages the iterative refinement process of diffusion models to synthesize lesions with natural tissue boundaries, preserved cellular structures, and authentic staining characteristics. We validate PathoGen across four diverse datasets representing distinct diagnostic challenges: kidney, skin, breast, and prostate pathology. Quantitative assessment confirms that PathoGen outperforms state-of-the-art generative baselines, including conditional GAN and Stable Diffusion, in image fidelity and distributional similarity. Crucially, we show that augmenting training sets with PathoGen-synthesized lesions enhances downstream segmentation performance compared to traditional geometric augmentations, particularly in data-scarce regimes. Besides, by simultaneously generating realistic morphology and pixel-level ground truth, PathoGen effectively overcomes the manual annotation bottleneck. This approach offers a scalable pathway for developing generalizable medical AI systems despite limited expert-labeled data.

## Introduction

The integration of artificial intelligence into histopathology has demonstrated remarkable potential for improving diagnostic accuracy, reducing pathologist workload, and enabling quantitative tissue analysis at unprecedented scales [1, 2]. Deep learning models have achieved expert-level performance in detecting malignancies [3], predicting treatment responses [4], and discovering novel prognostic biomarkers [5]. However, the development of robust, generalizable AI systems for histopathology remains fundamentally constrained by a critical challenge: the scarcity of expertly annotated training data, particularly for rare pathologies, early-stage lesions, and diagnostically challenging cases [6, 7].

Unlike natural image datasets where millions of labeled examples are readily available, histopathology suffers from inherent data limitations. Pixel-level annotation of tissue lesions requires extensive domain expertise, with pathologists spending hours delineating complex

morphological structures at cellular resolution [8]. This annotation burden is compounded by patient privacy concerns, institutional data silos, and the rarity of certain disease presentations—some pathological subtypes may have only dozens of documented cases worldwide [9]. Consequently, AI models trained on limited datasets exhibit poor generalization to new institutions, staining protocols, and patient populations, creating a significant barrier to clinical deployment [10].

Data augmentation has emerged as a cornerstone strategy for mitigating data scarcity in medical imaging [11]. Traditional geometric transformations—rotation, flipping, scaling, and color jittering—have shown modest improvements in model robustness [12]. However, these approaches merely recombine existing visual information without introducing novel pathological variations. They cannot generate new lesion morphologies, synthesize rare disease presentations, or create examples that bridge gaps in the training distribution. This limitation is particularly acute in histopathology, where diagnostic features span multiple spatial scales from subcellular organelles to tissue architecture, and where subtle morphological variations carry critical clinical significance [13, 14].

Recent advances in generative modeling offer a promising avenue for synthetic data generation. Generative Adversarial Networks (GANs) have been applied to histopathology image synthesis [15, 16], demonstrating the feasibility of creating visually plausible tissue images. However, GAN-based approaches face substantial challenges in this domain. Training instability often results in mode collapse, where generators produce limited diversity in lesion morphologies [17], which can manifest as artifacts at tissue boundaries and inconsistent staining patterns. Additionally, existing generative methods typically lack fine-grained control over lesion-specific attributes such as placement, size, and morphology—limiting their utility for targeted data augmentation in specific diagnostic scenarios [18].

Diffusion models have recently emerged as a powerful class of generative models that address many limitations of GANs [19]. By learning to iteratively denoise data through a reverse diffusion process, these models achieve superior sample quality, training stability, and mode coverage [20]. Diffusion models have demonstrated exceptional performance in natural image synthesis [21], medical image reconstruction [22], and various image-to-image translation tasks [23]. Their iterative refinement process is particularly well-suited for generating fine-grained details—a critical requirement for histopathology where diagnostic decisions depend on subcellular features. Moreover, recent work on conditional diffusion models has shown that spatial control can be achieved through various conditioning mechanisms [24-26], suggesting their potential for controllable lesion synthesis.

Despite these promising characteristics, diffusion models remain largely unexplored for histopathology data augmentation. Existing applications have focused primarily on reconstruction tasks [27] or unconditional whole-image generation [28], rather than the targeted, controllable lesion inpainting required for effective augmentation. The challenge lies in developing conditioning strategies that enable precise spatial control over lesion placement while ensuring that generated lesions exhibit natural integration with surrounding benign tissue, maintain realistic cellular morphology, and preserve tissue-specific architectural patterns.

Here we introduce PathoGen, a diffusion-based generative model specifically designed for controllable lesion inpainting in histopathology images. PathoGen takes as input a benign tissue image and a spatial mask indicating the desired lesion location, then synthesizes a realistic lesion within the specified region while maintaining seamless integration with surrounding tissue. We demonstrate PathoGen’s effectiveness across four diverse histopathology datasets representing clinically important diagnostic challenges: kidney glomeruli (glomerular disease detection), melanoma tumors (skin cancer diagnosis), breast invasive tumors (breast cancer subtyping), and prostate glands (prostate cancer grading). These datasets span different tissue types and diagnostic tasks, providing a rigorous test of generalization. When PathoGen-generated synthetic images are used to augment training data for lesion segmentation models, we observe consistent and substantial improvements in segmentation accuracy across all tissue types, with the most pronounced gains in low-data regimes where manual annotation is most resource-intensive. Notably, PathoGen automatically provides pixel-level annotations for all generated lesions, simultaneously addressing both data scarcity and annotation cost—two critical bottlenecks in computational pathology development.

## Methods

### Preliminaries

PathoGen is based on the Latent Diffusion Model (LDM) framework [29], which synthesizes high-resolution images by operating in a compressed latent space. It combines a pre-trained Variational Autoencoder (VAE) and a denoising U-Net, denoted as  $\epsilon_\theta(\cdot, t)$ . The VAE consists of an encoder  $E$  and a decoder  $D$ , which map between the image and latent spaces. Given an image  $x$ , the latent representation is computed as  $z_0 = E(x)$ . During training, Gaussian noise  $\epsilon \sim \mathcal{N}(0, I)$  is added to simulate the forward diffusion process, yielding a noisy latent  $z_t$ . The model is trained to denoise  $z_t$  by minimizing the standard LDM objective:

$$\mathcal{L}_{\text{LDM}} := \mathbb{E}_{z_0=E(x), \epsilon \sim \mathcal{N}(0, I), t} [\|\epsilon - \epsilon_\theta(z_t, t)\|_2^2]$$

Through iterative denoising, the model learns to reverse the diffusion process and generate meaningful latent representations, which are then decoded to image space via  $D(z_0)$ .

### Architecture and Training Strategy

PathoGen employs a shared VAE encoder for both benign tissue and lesion reference patches, ensuring that all inputs are embedded within a unified latent space to enable coherent integration during synthesis (Figure 1). Inspired by recent advances demonstrating the effectiveness of simple concatenation-based conditioning in diffusion models, we adopt a similar strategy that leverages direct visual feature fusion without relying on additional modality-specific encoders [30]. This architectural choice not only reduces the overall parameter count—leading to improved training efficiency and memory usage—but also facilitates spatial and structural consistency across modalities. In addition, unlike text-to-image generation tasks that necessitate cross-modal semantic alignment, our task demands pixel-level spatial coherence between input tissue image and inpainted pathological structures. Therefore, we remove cross-attention modules and text encoders entirely, as textual conditioning is

unnecessary for lesion inpainting where all relevant information is contained within the visual inputs.

To address the scarcity of paired benign-lesion datasets in histopathology, PathoGen adopts a self-supervised training strategy based on inpainting. The model learns to reconstruct randomly masked regions of real histopathology images without requiring explicit lesion annotations. For each  $1024 \times 1024$  image patch  $I \in \mathbb{R}^{3 \times H \times W}$ , a random arbitrary region is selected and expanded by a margin  $\delta \sim \mathcal{U}(50,200)$  pixels in all directions to create the final inpainting mask. This gap between the original region and the visible mask boundary encourages the model to synthesize smooth, natural transitions at lesion boundaries and prevents overfitting to edge pixels, thereby avoiding trivial reconstructions. To enable dynamic control during inference, classifier-free guidance [31] is incorporated into training. With a probability of 10%, conditional inputs (masked benign image and lesion reference) are replaced with learned null embeddings. This allows the model to operate both conditionally and unconditionally, facilitating inference-time guidance scaling.

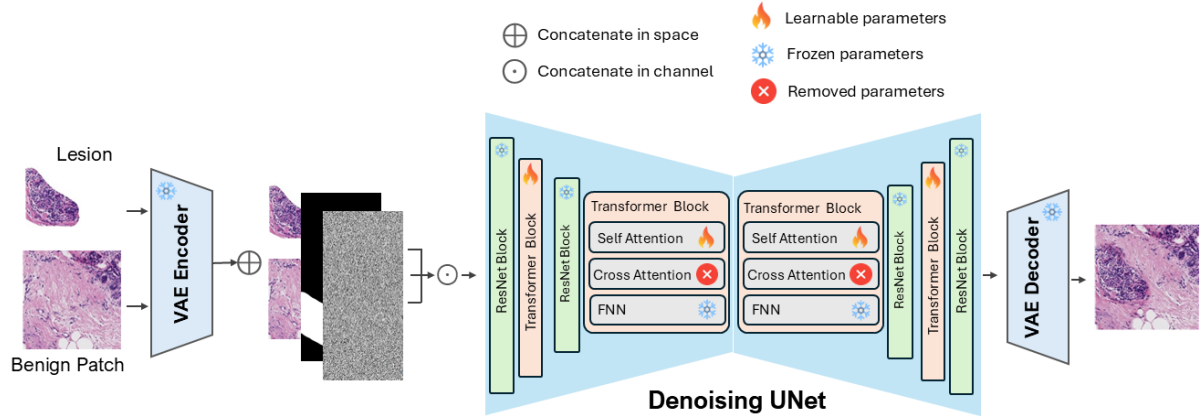


**Figure 1. Overview of the PathoGen architecture for lesion inpainting in histopathology images.** PathoGen spatially concatenates the benign tissue image with the lesion reference, ensuring they remain in the same latent feature space throughout the diffusion process. Only self-attention parameters providing global tissue-lesion interaction are learnable during training. Unnecessary cross-attention for text interaction is removed, and no additional conditions such as tissue segmentation are required. After denoising, the output latent is decoded back into image space using a frozen VAE decoder. The final output is a high-fidelity histopathology image with a synthesized lesion that is seamlessly integrated into the surrounding tissue.

## Implementation Details

We train PathoGen on histopathology image patches with resolution  $1024 \times 1024$  pixels, extracted from whole slide images (WSIs) scanned at  $40\times$  magnification. The model is trained for 100,000 iterations with a batch size of 8 using the AdamW optimizer with initial learning rate  $1 \times 10^{-5}$  and weight decay coefficient  $1 \times 10^{-2}$ . We employ a cosine annealing learning rate schedule with 5,000 warmup iterations, gradually increasing the learning rate from 0 to the initial value during warmup before following a cosine decay. Training is distributed across 4 NVIDIA RTX 6000 GPUs, requiring approximately 48 hours.

## Inference Process

PathoGen streamlines the inference process by requiring only a benign histopathology image, a lesion reference, and a target lesion mask—no preprocessing or extra conditioning is needed. Given a benign image  $I_b \in \mathbb{R}^{3 \times H \times W}$  and a binary mask  $M \in \mathbb{R}^{H \times W}$  specifying the lesion placement, we create a masked benign image  $I_{mas}$ :

$$I_m = I_b \otimes (1 - M)$$

where  $\otimes$  denotes the element-wise (Hadamard) product. The masked benign image  $I_m$  and lesion reference  $I_l \in \mathbb{R}^{3 \times H \times W}$  (e.g., a patch from another image with the target lesion type) are encoded into latents via the VAE encoder  $E$ :

$$X_m = E(I_m) \quad X_l = E(I_l)$$

where  $X_m, X_l \in \mathbb{R}^{4 \times \frac{H}{8} \times \frac{W}{8}}$ . The mask  $M$  is also interpolated to match the size of the latent space, resulting in  $m \in \mathbb{R}^{\frac{H}{8} \times \frac{W}{8}}$ . These are then concatenated spatially to form  $X_c \in \mathbb{R}^{8 \times \frac{H}{8} \times \frac{W}{8}}$  and  $m_c \in \mathbb{R}^{8 \times \frac{H}{8} \times \frac{W}{8}}$ :

$$X_c = X_m \oplus X_l, m_c = m \oplus O, \quad (4)$$

where  $\oplus$  indicates spatial concatenation, and  $O$  is an all-zero mask. This method maintains positional alignment between the benign context and lesion reference, guiding the model on lesion placement. The denoising begins with  $X_c$ ,  $m_c$ , and initial noise  $z_T \sim \mathcal{N}(0, 1)$  of matching size, concatenated channel-wise and fed into the UNet to predict  $z_{T-1}$ . This iterates over  $T$  timesteps to yield  $z_0$ . For timestep  $t$ :

$$z_{t-1} = \text{UNet}(z_t \odot m_c \odot X_c), \quad (5)$$

where  $\odot$  denotes channel-wise concatenation. The final  $z_0 \in \mathbb{R}^{8 \times \frac{H}{8} \times \frac{W}{8}}$  is split spatially to isolate the benign part  $z_0^b \in \mathbb{R}^{4 \times \frac{H}{8} \times \frac{W}{8}}$ , which is decoded via  $D$  to produce the output image  $\tilde{I}_b \in \mathbb{R}^{3 \times H \times W}$  with the inpainted lesion.

## Datasets

We train and evaluate PathoGen across four diverse histopathology datasets representing distinct tissue types, pathological conditions, and diagnostic challenges. The TIGER dataset [32] comprises digital pathology images of HER2-positive and triple-negative breast cancer (TNBC) whole-slide images with expert annotations of tissue compartments, lymphocytes, and plasma cells. The KPI dataset [33] addresses chronic kidney disease (CKD) through Periodic acid-Schiff (PAS) stained whole-slide images containing annotated glomeruli. The PUMA dataset [34] includes regions of interest from both primary and metastatic melanoma scanned at high magnification. The RING dataset [35] focuses on prostate gland segmentation in histopathological images, encompassing both healthy and pathological structures with varying degrees of glandular degeneration. For each dataset, we reserved 20% of whole-slide images as a held-out test set to evaluate model performance on completely unseen cases. From the remaining 80% of slides, we extracted  $1024 \times 1024$  pixel non-overlapping patches to create our training corpus. This split strategy ensures that test images come from different patients and slides than those used during training, providing a rigorous assessment of generalization

capability. We made 10,000 training patches from each dataset using arbitrary inpainting masks with randomly varying shapes, sizes, and positions to ensure diverse lesion synthesis scenarios.

## Results

### PathoGen produces more realistic and histologically accurate lesion inpainting

To evaluate the quality and realism of lesion synthesis, we compared PathoGen against two state-of-the-art generative baselines: CGAN (Conditional Generative Adversarial Network) [36] and StableDiffusion 1.5 [29]. We assessed performance through both quantitative metrics and qualitative visual inspection across all four histopathology datasets.

**Table 1. Quantitative evaluation of lesion synthesis quality.**

| <b>Method</b>   | <b>KPI</b>   |              | <b>TIGER</b> |              | <b>RING</b>  |              | <b>PUMA</b>  |              |
|-----------------|--------------|--------------|--------------|--------------|--------------|--------------|--------------|--------------|
|                 | <b>FID ↓</b> | <b>KID ↓</b> |
| CGAN            | 16.11        | 5.25         | 17.41        | 5.87         | 11.64        | 4.15         | 12.54        | 4.55         |
| StableDiffusion | 9.55         | 2.55         | 8.67         | 1.90         | 7.35         | 2.98         | 7.88         | 2.01         |
| <b>PathoGen</b> | <b>7.45</b>  | <b>1.23</b>  | <b>6.25</b>  | <b>0.92</b>  | <b>6.58</b>  | <b>1.88</b>  | <b>5.89</b>  | <b>1.11</b>  |

### *Quantitative Evaluation*

We employed two complementary image quality metrics to quantitatively assess the fidelity of generated lesions (Table 1). The Fréchet Inception Distance (FID) [37] measures the distributional similarity between generated and real images in feature space, with lower values indicating better quality and diversity. The Kernel Inception Distance (KID) [38] provides an unbiased estimate of the squared Maximum Mean Discrepancy between feature distributions, offering robust performance even with limited sample sizes. PathoGen consistently outperformed both baseline methods across all datasets and metrics, demonstrating superior image quality and distributional fidelity. Across the four tissue types, PathoGen achieved substantially lower FID and KID scores compared to both CGAN and StableDiffusion. The improvements were particularly pronounced when compared to CGAN, with PathoGen showing approximately 2-3× better performance on FID metrics and 3-5× improvement on KID metrics across datasets. When compared to StableDiffusion, PathoGen demonstrated consistent but more modest improvements. These quantitative improvements demonstrate that PathoGen generates lesions that more closely match the statistical distribution of real histopathology images, suggesting better preservation of tissue-specific features and morphological characteristics. The consistent superiority across diverse tissue types—from kidney glomeruli to breast tumors—indicates that PathoGen’s architecture effectively captures the unique morphological requirements of different histopathological contexts.

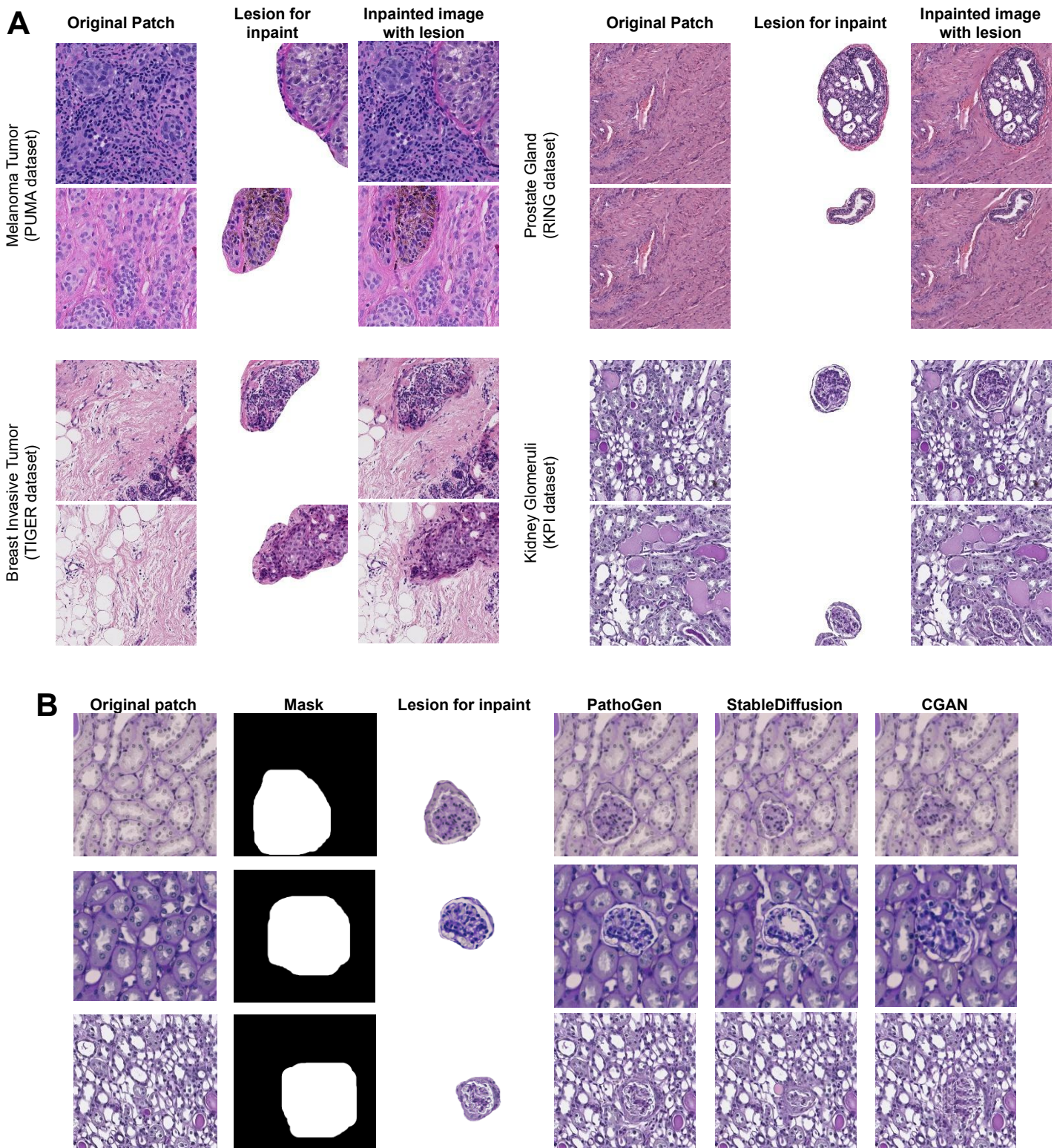


**Figure 2. PathoGen generates high-quality lesion inpainting across diverse histopathology datasets.** (A) Examples of PathoGen lesion synthesis across four tissue types showing original patches, lesion masks, and inpainted results. (B) Side-by-side comparison of PathoGen, StableDiffusion, and CGAN on kidney glomeruli examples. PathoGen produces more realistic tissue architecture and seamless boundary integration than baseline methods.

### *Qualitative Assessment*

Visual inspection of generated lesions revealed substantial qualitative differences between PathoGen and baseline approaches across multiple tissue types (Figure 2).

*PathoGen performance across diverse tissue types.* Figure 2A demonstrates PathoGen's ability to generate high-fidelity lesion inpainting across four distinct histopathology datasets. For the PUMA melanoma dataset, PathoGen successfully synthesized lesions with natural cellular density and preserved nuclear morphology characteristic of melanocytic proliferations. On the RING prostate dataset, the model generated glands with realistic lumen formation, appropriate epithelial layering, and natural stromal interfaces. For the TIGER breast cancer dataset, PathoGen inpainted tumor regions maintaining complex spatial relationships between tumor cells, stromal components, and infiltrating lymphocytes, with natural nuclear pleomorphism and appropriate tissue density gradients. The KPI kidney dataset presented the most challenging synthesis task due to highly specialized glomerular architecture. PathoGen successfully generated lesions with preserved mesangial architecture, realistic capillary wall thickness, and natural Bowman's space relationships. Across all datasets, PathoGen demonstrated consistent performance handling diverse lesion sizes while maintaining tissue-specific staining characteristics and achieving seamless integration with surrounding tissue.

*Comparative analysis with baseline methods.* Side-by-side comparisons with CGAN and StableDiffusion on representative kidney glomeruli examples (Figure 2B) revealed distinct performance differences across varying morphological challenges. PathoGen consistently generated lesions that closely matched the structural organization of reference lesions, preserving characteristic capillary tuft architecture, appropriate mesangial matrix distribution, and natural integration with surrounding tissue. The method successfully handled both intricate capillary loops and densely cellular regions, maintaining realistic nuclear spacing, appropriate chromatin distribution, and natural tissue density gradients throughout the lesions. In contrast, CGAN produced noticeable structural distortions across all examples, including loss of capillary loop definition, irregular cellular distribution, and color inconsistencies. CGAN particularly struggled with boundary regions, creating sharp discontinuities and color mismatches between inpainted lesions and surrounding tissue. StableDiffusion demonstrated intermediate performance, showing better structural preservation than CGAN but still exhibiting artifacts in mesangial regions, inconsistent cellular density patterns, and subtle boundary imperfections.

A key advantage of PathoGen was its superior handling of tissue boundaries and contextual integration. The inpainted lesions seamlessly blended with surrounding renal parenchyma, maintaining appropriate tissue proportions and natural interfaces without the sharp discontinuities or color mismatches frequently observed in baseline outputs. This seamless integration is critical for histopathology applications, as abrupt boundaries would be readily identified as artifacts by pathologists and could confound downstream diagnostic models. Furthermore, PathoGen demonstrated more consistent preservation of fine-grained morphological details including nuclear characteristics, cytoplasmic features, and extracellular matrix organization across diverse lesion types and tissue contexts.

## Synthetic lesions from PathoGen improve segmentation performance

To evaluate the practical utility of PathoGen-generated lesions, we assessed whether augmenting training datasets with synthetic samples could enhance downstream segmentation task performance. We trained UNet segmentation models on two conditions: (1) original datasets only (50 original patches), and (2) datasets augmented with PathoGen-generated lesions (50 original + 150 synthetic), then compared their segmentation accuracy using the Dice score metric. Across all four tissue types, models trained with PathoGen-augmented datasets demonstrated substantial performance improvements compared to baseline models trained on original data alone (Figure 3). For kidney glomeruli segmentation, the augmented model achieved a Dice score of 0.66 compared to 0.48 for the baseline, representing a notable improvement in segmentation accuracy. Similarly, melanoma tumor segmentation improved from 0.38 to 0.56 with PathoGen augmentation. Breast invasive tumor segmentation showed enhancement from 0.36 to 0.60, while prostate gland segmentation improved from 0.44 to 0.65. The consistent performance enhancement across all datasets demonstrates that PathoGen generates lesions that are not only visually realistic but also contain meaningful morphological information that benefits downstream computational pathology tasks. By augmenting limited training datasets with high-quality synthetic lesions, PathoGen addresses a critical challenge in computational pathology where annotated data is scarce and expensive to obtain.

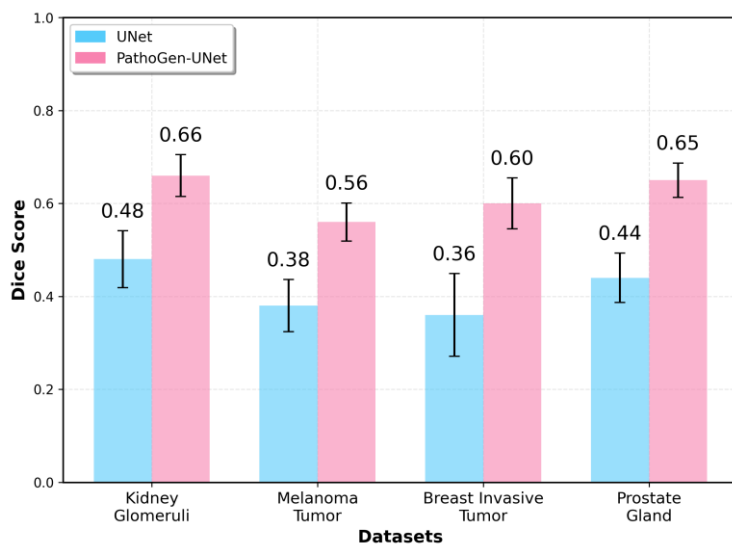


**Figure 3. Data augmentation with PathoGen-generated lesions enhances segmentation accuracy.** Comparison of UNet segmentation performance using Dice scores for models trained on original data only (50 patches, blue) versus PathoGen-augmented datasets (200 patches total, pink) across four tissue types.

## PathoGen enables effective data augmentation in low-data regimes

The true value of data augmentation emerges most clearly in data-scarce scenarios, where limited training examples constrain model performance. To evaluate PathoGen's effectiveness across the data availability spectrum, we conducted learning curve experiments, training models with varying amounts of real data (50, 100, 150, and 200 samples) with and without PathoGen augmentation.

Figure 4 presents learning curves for all four tissue types, plotting Dice score as a function of the number of real training samples. PathoGen-augmented models (shown in red) consistently outperform baseline models (shown in green) across all data regimes and tissue types. The performance gap between augmented and baseline models is most pronounced at small sample sizes and gradually narrows as more real data becomes available, confirming that synthetic augmentation provides maximum value precisely where it is needed most—in low-data regimes where acquiring additional annotated samples is most challenging and expensive.

Notably, the magnitude and persistence of improvements varied across tissue types. Some tissues, such as breast invasive tumor, maintained substantial performance gaps even at the highest data volumes, suggesting that PathoGen provides complementary morphological diversity beyond what is captured in the original dataset. In tissues like kidney glomeruli and prostate gland, the advantage of PathoGen augmentation decreased with more training data, confirming that synthetic augmentation is most valuable when real annotated samples are limited.

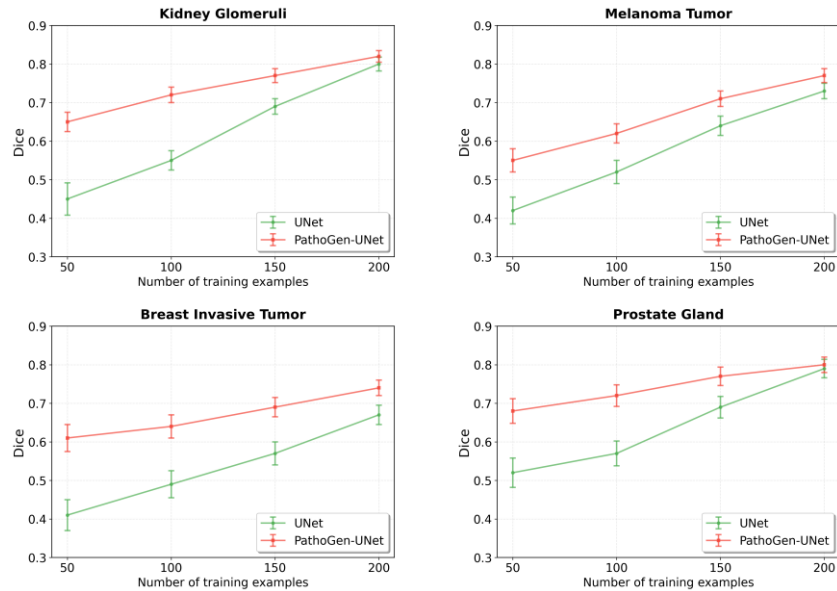


**Figure 4. Learning curves showing PathoGen's advantage in data-limited scenarios.** Segmentation performance (Dice score) versus number of real training samples for baseline UNet (green) and PathoGen-augmented UNet (red) across four tissue types. PathoGen augmentation provides consistent improvements, with largest gains at smaller sample sizes.

### Morphological augmentation outperforms geometric transformations

To evaluate the efficacy of PathoGen, we benchmarked its performance against a comprehensive set of baseline augmentation methods, encompassing both traditional geometric transformations (rotation, flipping, translation, and their combinations) and state-of-the-art generative models, including Conditional GAN (CGAN) and Stable Diffusion. All augmentation strategies were applied under identical experimental conditions: each method augmented a common base dataset of 50 real histopathology patches with 150 synthetic samples, which were then used to train UNet segmentation models.

As illustrated in Figure 5, PathoGen consistently achieved the highest segmentation performance across all four tissue types, significantly outperforming both traditional augmentations and competing generative approaches. While generative models (CGAN and Stable Diffusion) demonstrated moderate improvements over traditional methods, they still lagged behind PathoGen. This performance gap likely stems from the generative models' limited spatial control and insufficient awareness of tissue context during lesion synthesis, leading to synthetic samples that often lack the intricate histological coherence necessary for effective model training.

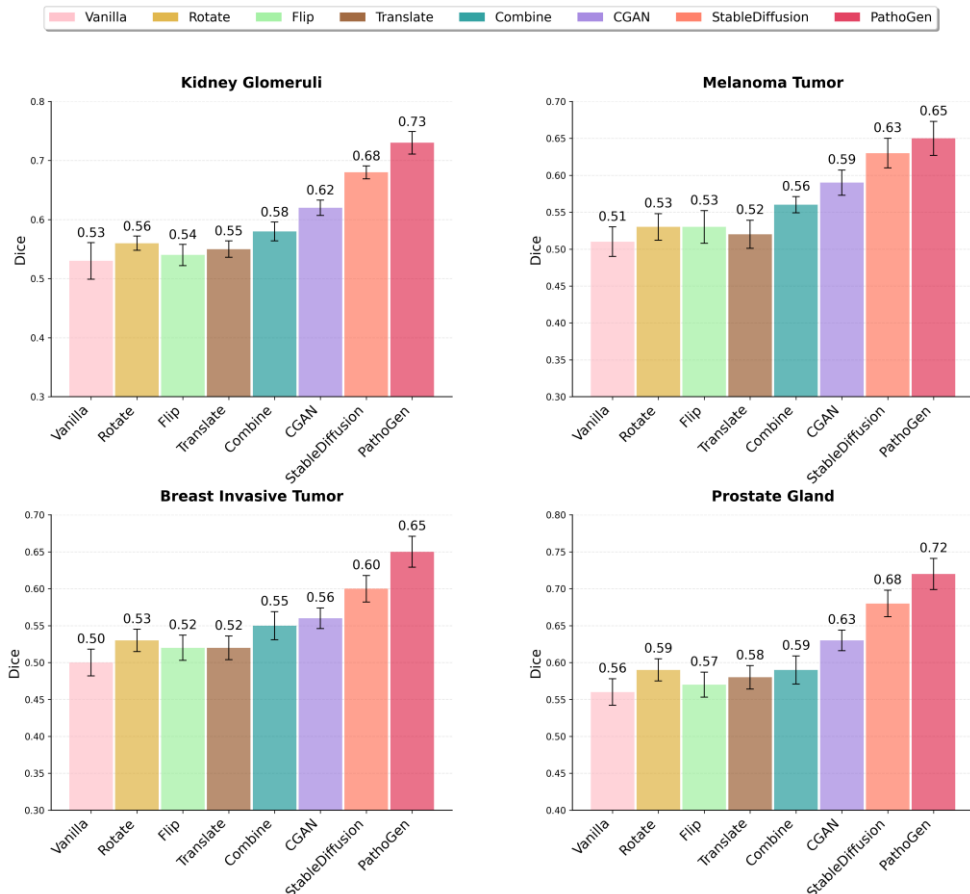


**Figure 5. Segmentation performance comparison across augmentation methods.** Dice scores for models trained with different augmentation approaches on four tissue types. All methods used 50 real patches plus 150 synthetic samples. PathoGen consistently outperforms traditional geometric augmentations (vanilla through combine), CGAN, and Stable Diffusion.

Traditional geometric augmentations yielded modest gains relative to training on unaugmented data. Among these, rotation consistently led to the most noticeable improvements in average Dice scores, with flipping and translation providing smaller incremental benefits. Combining multiple geometric transformations sequentially further enhanced performance, but the overall improvements remained substantially lower than those achieved with PathoGen. These findings highlight the inherent limitations of geometric augmentations in the context of

complex histopathology segmentation tasks. The limited effectiveness of geometric augmentations likely stems from their inability to generate novel pathological variations.

## Discussion

### **PathoGen addresses the dual bottleneck of data scarcity and annotation cost in computational pathology**

This study introduces PathoGen, a diffusion-based generative model that addresses a fundamental challenge in computational pathology: the scarcity of expert-annotated training data for AI model development. Our results demonstrate that PathoGen generates high-fidelity lesion inpainting across diverse tissue types while maintaining realistic cellular architectures, natural tissue boundaries, and authentic staining characteristics. When used for data augmentation, PathoGen-generated synthetic lesions consistently improve downstream segmentation performance across four clinically relevant histopathology datasets, with the most substantial gains observed in low-data regimes where acquiring additional annotations is most challenging [39].

A key practical advantage of PathoGen is that since inpainted lesion regions are defined by known masks, the model automatically provides pixel-level annotations for each generated patch. This capability enables the generation of large numbers of diverse, fully-annotated training samples without the need for manual expert annotation—a process that typically requires hours of pathologist time per image [40]. By simultaneously generating both synthetic images and their corresponding ground-truth annotations, PathoGen addresses the dual challenge of data scarcity and annotation cost that constrains AI development in computational pathology [41].

The superiority of PathoGen over existing approaches stems from several key advantages inherent to diffusion-based architectures. Unlike GANs, which suffer from training instability and mode collapse [42], the iterative refinement process of diffusion models enables more stable training and broader coverage of the morphological feature space [20]. This translates to greater diversity in generated lesion morphologies and more consistent preservation of fine-grained histological details. Furthermore, PathoGen's conditioning mechanism provides precise spatial control over lesion placement while ensuring contextual awareness of surrounding tissue—a critical requirement for generating lesions that seamlessly integrate with benign parenchyma. Our comparative analysis reveals that while general-purpose diffusion models like Stable Diffusion demonstrate reasonable performance, PathoGen's domain-specific architecture and training strategy yield substantially better results, highlighting the importance of tailoring generative models to the unique requirements of histopathology [43].

### **Morphological augmentation captures tissue-specific constraints that geometric transformations cannot represent**

Our comparative analysis against traditional geometric transformations reveals fundamental limitations of conventional augmentation approaches in histopathology [12]. While rotation, flipping, and translation provide modest performance gains, they cannot generate novel morphological variations or bridge gaps in the training distribution. This limitation is

particularly acute in histopathology where diagnostic features span multiple spatial scales and subtle morphological variations carry critical clinical significance. PathoGen, in contrast, synthesizes entirely new lesion instances with realistic cellular arrangements, appropriate nuclear characteristics, and natural tissue architecture—generating morphological diversity that extends beyond simple recombinations of existing visual information.

The superiority of morphological augmentation over geometric transformations also reflects the inherent properties of histopathological images. Unlike natural images where objects can appear at arbitrary orientations and scales, tissue architecture exhibits strong spatial priors and anatomical constraints [44]. Glomerular capillary loops, glandular lumens, and tumor-stromal interfaces follow characteristic organizational patterns that are not fully captured by simple geometric transformations. PathoGen's learned generative process respects these tissue-specific constraints while introducing biologically plausible variations, resulting in synthetic samples that better represent the true distribution of pathological presentations.

### **Computational efficiency and expert validation remain key challenges for clinical translation**

Despite promising results, two key limitations should be addressed in future work. First, computational requirements for diffusion-based generation exceed those of traditional augmentation approaches. PathoGen requires approximately 12 seconds per  $1024 \times 1024$  patch on a modern NVIDIA RTX6000 GPU, compared to milliseconds for geometric transformations. While this overhead is negligible compared to expert annotation time (which typically requires hours per whole-slide image), it may constrain real-time augmentation during training or deployment in computational resource-limited settings. Future work exploring distillation techniques [45] or accelerated sampling methods [45] could mitigate this limitation while preserving generation quality.

Second, our validation relied primarily on downstream segmentation performance and quantitative image quality metrics. While these measures provide objective assessment of distributional fidelity and practical utility, they may not fully capture diagnostic authenticity from expert pathologists' perspective [46]. Comprehensive reader studies with board-certified pathologists evaluating whether synthetic images contain diagnostically misleading features or artifacts would strengthen validation and build confidence for clinical translation. Future work should include blinded studies where pathologists assess the realism of generated lesions, their distinguishability from real tissue samples, and their fidelity to known pathological presentations. Such human expert evaluation would also help identify tissue-specific artifacts or systematic biases in the generation process that quantitative metrics might miss.

### **Conclusion**

PathoGen demonstrates that diffusion-based generative models, when fine-tuned for domain-specific histopathology images, can effectively address data scarcity challenges through controllable, high-fidelity image synthesis. By generating realistic lesions that preserve complex tissue architectures and seamlessly integrate with surrounding parenchyma, PathoGen enables substantial improvements in downstream segmentation tasks, particularly in low-data

regimes where manual annotation is most challenging. The consistent performance across diverse tissue types and superiority over both traditional augmentation methods and alternative generative approaches establish PathoGen as a promising tool for enhancing AI model development in histopathology. As computational pathology continues advancing toward clinical deployment, methods like PathoGen that can efficiently generate high-quality training data while respecting the unique morphological complexity of tissue images will play an increasingly important role in developing robust, generalizable diagnostic AI systems.

### Conflict of interest

The authors of this study declare that they do not have any conflict of interest.

### Data availability statement

The data we used are publicly available and have already been referenced in our manuscript. The training and inference code is available at <https://github.com/mkoohim/PathoGen>. Additionally, the fine-tuned model weights are available on our Hugging Face page: <https://huggingface.co/mkoohim/PathoGen>.

### Funding

There is no funding for this project.

### References:

- [1] C. D. Bahadir *et al.*, "Artificial intelligence applications in histopathology," *Nature Reviews Electrical Engineering*, vol. 1, no. 2, pp. 93-108, 2024.
- [2] A. Shmatko, N. Ghaffari Laleh, M. Gerstung, and J. N. Kather, "Artificial intelligence in histopathology: enhancing cancer research and clinical oncology," *Nature cancer*, vol. 3, no. 9, pp. 1026-1038, 2022.
- [3] A. B. Hamida *et al.*, "Deep learning for colon cancer histopathological images analysis," *Computers in Biology and Medicine*, vol. 136, p. 104730, 2021.
- [4] D.-T. Hoang *et al.*, "A deep-learning framework to predict cancer treatment response from histopathology images through imputed transcriptomics," *Nature cancer*, vol. 5, no. 9, pp. 1305-1317, 2024.
- [5] D. Mandair, J. S. Reis-Filho, and A. Ashworth, "Biological insights and novel biomarker discovery through deep learning approaches in breast cancer histopathology," *NPJ breast cancer*, vol. 9, no. 1, p. 21, 2023.
- [6] J. Wei *et al.*, "Learn like a pathologist: curriculum learning by annotator agreement for histopathology image classification," in *Proceedings of the IEEE/CVF winter conference on applications of computer vision*, 2021, pp. 2473-2483.
- [7] M. Cooper, Z. Ji, and R. G. Krishnan, "Machine learning in computational histopathology: Challenges and opportunities," *Genes, Chromosomes and Cancer*, vol. 62, no. 9, pp. 540-556, 2023.
- [8] D. Montezuma *et al.*, "Annotation practices in computational pathology: a European Society of Digital and Integrative Pathology (ESDIP) survey study," *Laboratory Investigation*, vol. 105, no. 3, p. 102203, 2025.

- [9] C. Siech *et al.*, "Rare histological prostate cancer subtypes: Cancer-specific and other-cause mortality," *Prostate cancer and prostatic diseases*, vol. 28, no. 3, pp. 748-754, 2025.
- [10] H. Evans and D. Snead, "Why do errors arise in artificial intelligence diagnostic tools in histopathology and how can we minimize them?," *Histopathology*, vol. 84, no. 2, pp. 279-287, 2024.
- [11] T. Islam, M. S. Hafiz, J. R. Jim, M. M. Kabir, and M. Mridha, "A systematic review of deep learning data augmentation in medical imaging: Recent advances and future research directions," *Healthcare Analytics*, vol. 5, p. 100340, 2024.
- [12] T. Kumar, R. Brennan, A. Mileo, and M. Bendechache, "Image data augmentation approaches: A comprehensive survey and future directions," *IEEE Access*, 2024.
- [13] Y. Gao *et al.*, "Histology image analysis of 13 healthy tissues reveals molecular-histological correlations," *Scientific Reports*, vol. 15, no. 1, p. 26812, 2025.
- [14] L. Hou, A. Agarwal, D. Samaras, T. M. Kurc, R. R. Gupta, and J. H. Saltz, "Robust histopathology image analysis: To label or to synthesize?," in *Proceedings of the IEEE/CVF conference on computer vision and pattern recognition*, 2019, pp. 8533-8542.
- [15] S. A. Alajaji *et al.*, "Generative adversarial networks in digital histopathology: current applications, limitations, ethical considerations, and future directions," *Modern Pathology*, vol. 37, no. 1, p. 100369, 2024.
- [16] A. Das, V. K. Devarampati, and M. S. Nair, "NAS-SGAN: A semi-supervised generative adversarial network model for atypia scoring of breast cancer histopathological images," *IEEE Journal of Biomedical and Health Informatics*, vol. 26, no. 5, pp. 2276-2287, 2021.
- [17] M. E. Tschuchnig, G. J. Oostingh, and M. Gadermayr, "Generative adversarial networks in digital pathology: a survey on trends and future potential," *Patterns*, vol. 1, no. 6, 2020.
- [18] J. Hussain, M. Båth, and J. Ivarsson, "Generative adversarial networks in medical image reconstruction: A systematic literature review," *Computers in biology and medicine*, vol. 191, p. 110094, 2025.
- [19] P. Dhariwal and A. Nichol, "Diffusion models beat gans on image synthesis," *Advances in neural information processing systems*, vol. 34, pp. 8780-8794, 2021.
- [20] C. Oulmalme, H. Nakouri, and F. Jaafar, "A systematic review of generative AI approaches for medical image enhancement: Comparing GANs, transformers, and diffusion models," *International journal of medical informatics*, p. 105903, 2025.
- [21] M. Özbeý *et al.*, "Unsupervised medical image translation with adversarial diffusion models," *IEEE Transactions on Medical Imaging*, vol. 42, no. 12, pp. 3524-3539, 2023.
- [22] A. Kazerouni *et al.*, "Diffusion models in medical imaging: A comprehensive survey," *Medical image analysis*, vol. 88, p. 102846, 2023.
- [23] J. Kim and H. Park, "Adaptive latent diffusion model for 3d medical image to image translation: Multi-modal magnetic resonance imaging study," in *Proceedings of the IEEE/CVF Winter conference on applications of computer Vision*, 2024, pp. 7604-7613.
- [24] S. Zou *et al.*, "Towards efficient diffusion-based image editing with instant attention masks," in *Proceedings of the AAAI Conference on Artificial Intelligence*, 2024, vol. 38, no. 7, pp. 7864-7872.
- [25] B. Kawar *et al.*, "Imagic: Text-based real image editing with diffusion models," in *Proceedings of the IEEE/CVF conference on computer vision and pattern recognition*, 2023, pp. 6007-6017.

- [26] C. Corneau, R. Gadde, and A. M. Martinez, "Latentpaint: Image inpainting in latent space with diffusion models," in *Proceedings of the IEEE/CVF winter conference on applications of computer vision*, 2024, pp. 4334-4343.
- [27] C. Wang, Z. He, J. He, J. Ye, and Y. Shen, "Histology image artifact restoration with lightweight transformer based diffusion model," in *International Conference on Artificial Intelligence in Medicine*, 2024: Springer, pp. 81-89.
- [28] N. Sridhar, M. Elad, C. McNeil, E. Rivlin, and D. Freedman, "Diffusion models for generative histopathology," in *International Conference on Medical Image Computing and Computer-Assisted Intervention*, 2023: Springer, pp. 154-163.
- [29] R. Rombach, A. Blattmann, D. Lorenz, P. Esser, and B. Ommer, "High-resolution image synthesis with latent diffusion models," in *Proceedings of the IEEE/CVF conference on computer vision and pattern recognition*, 2022, pp. 10684-10695.
- [30] Z. Chong *et al.*, "Catvton: Concatenation is all you need for virtual try-on with diffusion models," *arXiv preprint arXiv:2407.15886*, 2024.
- [31] J. Ho and T. Salimans, "Classifier-free diffusion guidance," *arXiv preprint arXiv:2207.12598*, 2022.
- [32] grand-challenge.org. "TIGER - Grand Challenge." <https://tiger.grand-challenge.org/Home/> (accessed 2025).
- [33] R. Deng *et al.*, "Kpis 2024 challenge: Advancing glomerular segmentation from patch-to slide-level," *arXiv preprint arXiv:2502.07288*, 2025.
- [34] M. Schuivingel, H. Liu, and D. Eek, "A novel dataset for nuclei and tissue segmentation in Melanoma with baseline nuclei segmentation and tissue segmentation benchmarks.[DOME-ML Annotations]. 2025," ed.
- [35] M. Salvi *et al.*, "A hybrid deep learning approach for gland segmentation in prostate histopathological images," *Artificial Intelligence in Medicine*, vol. 115, p. 102076, 2021.
- [36] M. Mirza and S. Osindero, "Conditional generative adversarial nets," *arXiv preprint arXiv:1411.1784*, 2014.
- [37] M. Heusel, H. Ramsauer, T. Unterthiner, B. Nessler, and S. Hochreiter, "Gans trained by a two time-scale update rule converge to a local nash equilibrium," *Advances in neural information processing systems*, vol. 30, 2017.
- [38] G. Parmar, R. Zhang, and J.-Y. Zhu, "On aliased resizing and surprising subtleties in gan evaluation," in *Proceedings of the IEEE/CVF conference on computer vision and pattern recognition*, 2022, pp. 11410-11420.
- [39] L. Zhang *et al.*, "Generative AI enables medical image segmentation in ultra low-data regimes," *Nature Communications*, vol. 16, no. 1, p. 6486, 2025.
- [40] G. Cazzaniga *et al.*, "Improving the Annotation Process in Computational Pathology: A Pilot Study with Manual and Semi-automated Approaches on Consumer and Medical Grade Devices," *Journal of Imaging Informatics in Medicine*, vol. 38, no. 2, pp. 1112-1119, 2025.
- [41] B. R. Mitchell, M. C. Cohen, and S. Cohen, "Dealing with multi-dimensional data and the burden of annotation: easing the burden of annotation," *The American Journal of Pathology*, vol. 191, no. 10, pp. 1709-1716, 2021.
- [42] M. Durgadevi, "Generative Adversarial Network (GAN): A general review on different variants of GAN and applications," in *2021 6th International Conference on Communication and Electronics Systems (ICCES)*, 2021: IEEE, pp. 1-8.
- [43] J. S. Yoon, K. Oh, Y. Shin, M. A. Mazurowski, and H.-I. Suk, "Domain generalization for medical image analysis: A review," *Proceedings of the IEEE*, 2024.
- [44] P. Isnard, D. Li, Q. Xuanyuan, H. Wu, and B. D. Humphreys, "Histopathologic analysis of human kidney spatial transcriptomics data: toward precision pathology," *The American Journal of Pathology*, vol. 195, no. 1, pp. 69-88, 2025.

- [45] T. H. Nguyen and A. Tran, "Swiftbrush: One-step text-to-image diffusion model with variational score distillation," in *Proceedings of the IEEE/CVF Conference on Computer Vision and Pattern Recognition*, 2024, pp. 7807-7816.
- [46] M. Koohi-Moghadam and K. T. Bae, "Generative AI in medical imaging: applications, challenges, and ethics," *Journal of Medical Systems*, vol. 47, no. 1, p. 94, 2023.